

Modelling the fraction of Lyman Break Galaxies with strong Lyman- α emission at $5 \leq z \leq 7$

Jaime E. Forero-Romero¹ \star , Gustavo Yepes², Stefan Gottlöber¹
& Francisco Prada³

¹ *Leibniz-Institut für Astrophysik Potsdam (AIP), An der Sternwarte 16, 14482 Potsdam, Germany*

² *Grupo de Astrofísica, Universidad Autónoma de Madrid, Madrid E-28049, Spain*

³ *Instituto de Astrofísica de Andalucía (CSIC), Camino Bajo de Huétor 50, E-18008, Granada, Spain*

5 December 2018

ABSTRACT

We present theoretical results for the expected fraction of Lyman Break Galaxies (LBGs) to be detected as strong Lyman- α emitters (LAEs) in the redshift range $5 \leq z \leq 7$. We base our analysis on the 2-billion particle SPH simulation *MareNostrum High-z Universe*. We approximate galaxies as static dusty slabs with an additional clumpy dust distribution affecting stellar populations younger than 25 Myr. The model for the Lyman- α escape fraction is based on the results of our Monte-Carlo radiative transfer code (CLARA) for a slab configuration. We also fix the transmission of Lyman- α photons through the intergalactic medium to a constant value of 50% at all redshifts. From the results of this model we calculate $x_{\text{Ly}\alpha}$, the fraction of Lyman Break Galaxies with Ly α equivalent width (EW) larger than 50Å. We find a remarkable agreement with observational data at $4.5 < z < 6$. For bright ($-22 < M_{\text{UV}} < -20.5$) and faint ($-20.5 < M_{\text{UV}} < -18.5$) galaxies our model predicts $x_{\text{Ly}\alpha} = 0.02 \pm 0.01$ and $x_{\text{Ly}\alpha} = 0.47 \pm 0.01$ while observers report $x_{\text{Ly}\alpha} = 0.08 \pm 0.02$ and $x_{\text{Ly}\alpha} = 0.47 \pm 0.16$, respectively. Additional evolution of the extinction model at redshift $z \sim 7$, that decreases the intensity of transmitted Lyman- α radiation by a factor of $f_{\text{T}} = 0.4$ as to match the LAE luminosity function at $z \sim 6.5$, naturally provides a good match for the recently reported $x_{\text{Ly}\alpha}$ fractions at $z > 6.3$. Exploring different toy models for the Lyman- α escape fraction, we show that a decreasing Lyman- α escape fraction with increasing UV galaxy luminosity is a key element in our model to explain the trend of larger $x_{\text{Ly}\alpha}$ fractions for fainter LBGs.

Key words: galaxies: high-redshift — galaxies: evolution — methods: N-body simulations

1 INTRODUCTION

The study of distant star forming galaxies is being driven by even more sensitive observations. Observational samples are now commonly gathered both for Lyman Break Galaxies (LBG) and Lyman- α emitting (LAE) galaxies in the redshift range $z > 4$ (see Hayes et al. (2011) and references therein). Nevertheless, a clear physical connection between these two populations is difficult to establish given the complex physics involved in the transmission Lyman- α radiation in the interstellar medium (ISM) (Hansen & Oh 2006).

Recently, observational results have reported on the fraction of LBGs that show strong Lyman- α emission, $x_{\text{Ly}\alpha}$, at a given absolute rest-frame UV magnitude (Stark et al.

2010, 2011; Schenker et al. 2011). This fraction derived from observational data provides a simple test to theoretical models that seek to explain, under a sound physical model, the connection between LBGs and LAEs. Because this test is concerned with fractions of a population, it is largely insensitive to changes in absolute number densities of the observed galaxies, adding new information with respect to analysis based on the LAE luminosity function (LF).

In this paper we make theoretical predictions on the $x_{\text{Ly}\alpha}$ fraction as function of absolute rest-frame magnitude M_{UV} in the redshift range $5 \leq z \leq 7$. These results are based on a simulation of a cosmological volume that follows the dynamical evolution of roughly 2 billion dark matter and gas particles including star formation and supernovae feedback. The clumpy dust attenuation model and its effects on the UV luminosity function were de-

\star Email: jforero@aip.de

scribed in detail in Forero-Romero et al. (2010) (Paper I hereafter). The corresponding Lyman- α escape fraction is calculated using the results of our Monte-Carlo code **CLARA**. In Forero-Romero et al. (2011) (Paper II hereafter) we discussed at length the structure of the code and the implications for the luminosity functions in the redshift range $5 \leq z \leq 7$.

In Section 2 we describe the numerical simulation and the model for the UV/Lyman- α emission and its associated extinction/escape fraction. Next (§3) we describe the results of this model for the $x_{\text{Ly}\alpha}$ statistic in the redshift range $5 \leq z \leq 7$. We also explore different toy models for the Lyman α escape fraction in order to better understand the trends found in the simulation. We discuss the results in Section 4 and present our conclusions in Section 5.

2 A SIMULATION OF HIGH REDSHIFT LBGs AND LAES

The cosmological simulation, the algorithm of galaxy finding and the spectral modeling (UV continuum and Lyman- α line) have been thoroughly described in Paper I and II. Here we summarize the most relevant features for this Paper.

2.1 The MareNostrum High-Z Universe Simulation

The *MareNostrum High-z Universe* simulation¹ follows the non linear evolution of structures in baryons (gas and stars) and dark matter, starting from $z = 60$ within a cube of $50h^{-1}\text{Mpc}$ comoving on a side. The cosmological parameters used correspond to WMAP1 data (Spergel et al. 2003) and are $\Omega_m = 0.3$, $\Omega_b = 0.045$, $\Omega_\Lambda = 0.7$, $\sigma_8 = 0.9$, a Hubble parameter $h = 0.7$, and a spectral index $n = 1$. The initial density field has been sampled by 1024^3 dark matter particles with a mass of $m_{\text{DM}} = 8.2 \times 10^6 h^{-1} \text{M}_\odot$ and 1024^3 SPH gas particles with a mass of $m_{\text{gas}} = 1.4 \times 10^6 h^{-1} \text{M}_\odot$. The simulation has been performed using the TREEPM+SPH code **GADGET-2** (Springel 2005). The gravitational smoothing scale was set to $2 h^{-1} \text{kpc}$ in comoving coordinates. We follow Springel & Hernquist (2003) to model the cooling, star formation and strong kinetic feedback model in the form of galactic winds. We identify the objects in the simulations using the **AMIGA** Halo Finder (AHF) (Knollmann & Knebe 2009). All objects with more than 1000 particles, dark matter, gas and stars combined, are used in our present analyses. We assume a galaxy is resolved if the object contains 200 or more star particles, which corresponds to objects with $\gtrsim 400$ particles of gas.

2.2 UV and Lyman- α emission

The photometric properties of galaxies are calculated employing the stellar population synthesis model **STARDUST** (Devriendt et al. 1999). Using the methods described in Hatton et al. (2003).

We consider only the intrinsic Lyman- α emission associated to star formation. We assume that the number of Hydrogen ionizing photons per unit time is 1.8×10^{53} photons s^{-1} for a star formation rate of $1 \text{ M}_\odot/\text{yr}$ (Leitherer et al. 1999).

Assuming that 2/3 of these photons are converted to Lyman- α photons (case-B recombination, Osterbrock 1989), the intrinsic Lyman- α luminosity as a function of the star formation rate is

$$L_{\text{Ly}\alpha} = 1.9 \times 10^{42} \times (\text{SFR}/\text{M}_\odot \text{ yr}^{-1}) \text{ erg s}^{-1}. \quad (1)$$

A change in the escape fraction of ionizing photons can thus induce changes in the intrinsic Lyman- α emission. In our model, we take this ionizing photon escape fraction to be negligible.

2.3 Dust attenuation

Our approach to calculate the dust extinction is purely phenomenological. The extinction curve for each galaxy is different depending on its metallicity and gas contents (Guiderdoni & Rocca-Volmerange 1987). The dust attenuation model parametrizes both the extinction in a homogeneous ISM and in the molecular clouds around young stars, following the physical model of Charlot & Fall (2000). The attenuation from dust in the homogeneous ISM assumes a slab geometry, while the additional attenuation for young stars is modeled using spherical symmetry.

We first describe the optical depth for the homogeneous interstellar medium, denoted by $\tau_d^{\text{ISM}}(\lambda)$. We take the mean optical depth of a galactic disc at wavelength λ to be

$$\tau_d^{\text{ISM}}(\lambda) = \eta \left(\frac{A_\lambda}{A_V} \right)_{Z_\odot} \left(\frac{Z_g}{Z_\odot} \right)^r \left(\frac{\langle N_H \rangle}{2.1 \times 10^{21} \text{ atoms cm}^{-2}} \right), \quad (2)$$

where A_λ/A_V is the extinction curve from Mathis et al. (1983), Z_g is the gas metallicity, $\langle N_H \rangle$ is the mean atomic hydrogen column density and $\eta = (1+z)^{-\alpha}$ is a factor that takes into account the evolution of the dust to gas ratio at different redshifts.

The extinction curve depends on the gas metallicity Z_g and is based on an interpolation between the solar neighborhood and the Large and Small Magellanic Clouds ($r = 1.35$ for $\lambda < 2000 \text{\AA}$ and $r = 1.6$ for $\lambda > 2000 \text{\AA}$).

Stars younger than a given age, t_c , are subject to an additional attenuation in the birth clouds (BC) with optical depth

$$\tau_d^{\text{BC}}(\lambda) = \left(\frac{1}{\mu} - 1 \right) \tau_d^{\text{ISM}}(\lambda), \quad (3)$$

where μ is the fraction of the total optical depth for these young stars with respect to that is found in the homogeneous ISM.

2.4 Lyman- α escape fraction

In Paper II using our radiative transfer code **CLARA** we obtained the Lyman- α escape fraction for the corresponding slab described as a function of the product $(a\tau_0)^{1/3}\tau_a$,

¹ <http://astro.ft.uam.es/marenosttrum>

where τ_0 is the Hydrogen optical depth, τ_a is the optical depth of absorbing material (for albedo values of A , $\tau_a = (1 - A)\tau_d$, where τ_d is the dust optical depth), and a is a measure of the gas temperature defined as $a = \Delta\nu_L/(2\Delta\nu_D)$, $\Delta\nu_D = (v_p/c)\nu_0$ is the Doppler frequency width, and $v_p = (2kT/m_H)^{1/2}$ is $\sqrt{2}$ times the velocity dispersion of the Hydrogen atom, T is the gas temperature, m_H is the Hydrogen atom mass and $\Delta\nu_L$ is the natural line width.

We find that the equation

$$f_\alpha = \frac{1 - \exp(-P)}{P} \quad (4)$$

where

$$P = \epsilon((a\tau_0)^{1/3}\tau_a)^{3/4}, \quad (5)$$

with $\epsilon = 3.5$ provides a reasonable description of the Monte-Carlo results for $(a\tau_0)^{1/3}\tau_a < 200$ for the slab geometry with homogeneously distributed sources.

In addition to the foreground, homogeneous ISM extinction, we model the attenuation due to the birth clouds. Under the physical conditions for these poor neutral hydrogen clouds, $\tau_0^{BC} \sim \tau_a^{BC}$ together with $a\tau_0^{BC} < 1$ and furthermore $\tau_a^{BC} > 1$, the enhancement in absorption by resonant scattering becomes irrelevant. Under these conditions, we take the escape fraction as the continuum extinction at $\lambda = 1260\text{\AA}$ for a spherical geometry.

The effect of gas kinematics is not taken into account in the model. Appropriate outflow configurations can increase the Lyman- α escape fraction (Kunth et al. 1998; Verhamme et al. 2006; Atek et al. 2008).

2.5 Transmission through the IGM

In Paper II we assumed that the IGM allows the transmission of 50 per cent of the Lyman- α line at every redshift $5 \leq z \leq 7$. This is quantified by a transmission coefficient $\mathcal{T}_{\text{IGM}} = 0.50$, which can be considered optimistic given recent numerical estimations.

Simplified analytic modeling (Stark et al. 2011) of $\mathcal{T}_{\text{IGM}} = \exp(-\tau_\alpha)$ where τ_α is the optical depth for Lyman- α photons (calculated from Meiksin (2006)), yield $\mathcal{T}_{\text{IGM}} = 0.58$ and $\mathcal{T}_{\text{IGM}} = 0.51$ at redshifts $z \sim 5$ and $z \sim 6$. 3D Monte Carlo radiative transfer calculations of individual galaxies obtain values for the IGM transmission at $z \sim 6$ of $\mathcal{T}_{\text{IGM}} = 0.26_{-0.18}^{+0.13}$ (Laursen et al. 2011), a result that is readily explained by the effect of circumgalactic gas infall (Dijkstra et al. 2007; Iliev et al. 2008; Dayal et al. 2011). Radiative transfer calculations by Zheng et al. (2010) find both a larger scatter and a lower mean value in the fraction of intrinsic Lyman- α radiation effectively detected at $z \sim 6$. However, in that calculation the authors need to boost by a factor of ~ 5 the intrinsic Lyman- α intensity in order to match the observational constraints from the luminosity function.

Our model requires a transmission fraction ($\mathcal{T}_{\text{IGM}} = 0.5$) higher than the favored values for a symmetric Lyman- α line ($\mathcal{T}_{\text{IGM}} < 0.4$). Due to the degeneracy between the escape fraction and the IGM transmission (the observed Lyman- α luminosity is reduced by a factor $f_\alpha \times \mathcal{T}_{\text{IGM}}$) lower transmission fractions \mathcal{T}_{IGM} can be compensated by higher escape

fractions f_α . Given that the clumpiness and amount of dust is already fixed by the LBG modelling, the freedom of changing f_α is restricted. The most probable interpretation is that outflows have to be considered in order to provide a physical picture that explains the values of $\mathcal{T}_{\text{IGM}} \sim 0.5$ we need. As mentioned in the last section, outflows will also have an impact on the f_α escape fraction. Quantifying the effect of outflows is an issue we will address in the future using the tools and simulations presented in Paper I and Paper II.

At redshifts $z \gtrsim 6$, before reionization is completed, the estimations of the IGM transmission fraction depend on the assumptions made to model both the reionization and the Lyman- α line radiative transfer (McQuinn et al. 2007; Dayal et al. 2011; Dijkstra et al. 2011). This makes even more difficult to reach a conclusive prediction on the expected values for \mathcal{T}_{IGM} at a fixed redshift and will influence the interpretation of our results beyond $z > 6$, as will be discussed in Section 4.2.

2.6 Comparison with the observational Luminosity Functions

In Paper I we applied the above mentioned extinction model to match the rest-frame UV LFs derived from the simulation to the observed LFs in the redshift range $5 \leq z \leq 7$. The final model imposes additional extinction in all the stellar populations younger than $t_c = 25$ Myr, with parameters $\mu = 0.01$ for redshifts $z \sim 5, 6$ and $\mu = 0.03$ for redshift $z \sim 7$, and $\alpha = 1.5$. At the faint end ($M_{\text{UV}} < -20$) we have spotted a slight overabundance at all simulated redshifts that could hint towards a low efficiency in the supernovae feedback that can regulate the star formation process in the shallow potential wells of the corresponding halos with masses $\sim 2 \times 10^{10} h^{-1} M_\odot$.

In Paper II, with the dust contents already constrained from the UV LFs, we applied the model for the Lyman- α escape fraction to construct the LAE LFs. We note that the LAEs used to construct the LF had an equivalent width (EW) larger than a fiducial threshold of 20\AA , imposed to resemble a minimal threshold for observational detection. At redshifts $z \sim 5$ and $z \sim 6$ we found a good match at the bright-end within the Poissonian and cosmic variance uncertainties. The match with observations is also good if we consider IGM transmission fractions of 58 and 51 per cent as calculated by Stark et al. (2011) using the results by Meiksin (2006).

However, there is an excess at the faint end of the simulated LF with respect to the observations. The overabundance corresponds to luminosities of $L_{\text{Ly}\alpha} \sim 2 \times 10^{42}$ erg/s, where we found as well a mild overabundance at the faint end of the UV LFs, if the star formation is lowered in some of these numerical galaxies as to match the observed abundance, both the intrinsic UV and Lyman- α emission will drop, making the galaxies to fall below the detectable range. Therefore, this change will not bear strong consequences for the fraction $x_{\text{Ly}\alpha}$ because of the simultaneous changes in LBGs and LAEs abundance.

At redshift $z \sim 7$ the normalization of the LAE LF is still higher than observed at all luminosities by a factor of ~ 0.4 in luminosity. By dimming each LAE in the simulation by a factor of $f_T = 0.4$ we can reproduce the LF abundances at $z \sim 6.5$ (Kashikawa et al. 2006).

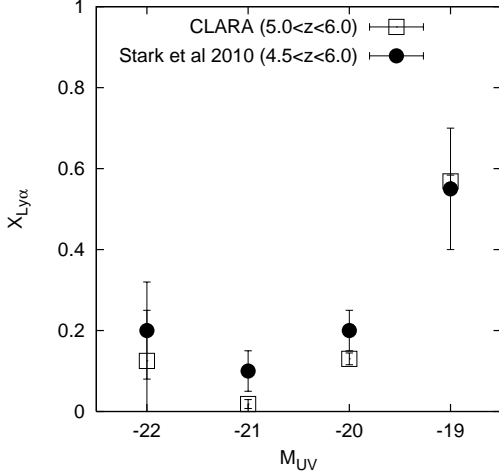


Figure 1. Fraction of galaxies showing strong Lyman- α emission as a function of the absolute M_{UV} magnitude in the models (empty symbols) and observations (filled circles). The error bars in the model are calculated from the Poissonian variance on the number of strong emitting LAEs. The results of our model (squares) in the redshift range $5 \leq z \leq 6$ shows a broad agreement with the observations reported by Stark et al. (2010, 2011).

3 RESULTS

3.1 Lyman- α fraction at $5 < z < 7$

For each well resolved galaxy in the three simulation snapshots at $z = 5, 6, 7$ we calculate the UV magnitudes corrected by dust absorption, M_{UV} , the slopes of the spectra between 1200 Å and 1600 Å, β , together with the intrinsic and observed Lyman- α luminosities. Then, for each galaxy we calculate the continuum flux red-wards of the Lyman- α line at 1240 Å from the β slope values and the flux calculated from the M_{UV} magnitudes. This way of calculating the continuum was chosen to mimic the method used in Stark et al. (2010). The Lyman- α EW is then calculated as the ratio of the observed intensity in the Lyman- α line and the UV continuum.

We then bin the galaxies in M_{UV} and calculate the fraction of LBGs with Lyman- α EW larger than 50 Å. In Fig 1 we plot the fraction of galaxies with strong Lyman- α emission ($x_{Ly\alpha}$) at redshifts $z = 5$ and $z = 6$ combined, and compared to the observational results at $4.5 < z < 6.0$. As can be clearly seen in the plot, we are able to reproduce the observational trend without any fine-tuning of our simulated galaxies. Namely the values of $x_{Ly\alpha}$ for the bright LBGs with $M_{UV} < -20.5$ and the increase in the fraction of LAEs for faint LBGs with $M_{UV} > -20.5$. The upturn in $x_{Ly\alpha}$ around $M_{UV} = -21.0$ is also reproduced, which is a consequence of reproducing the shape of the UV LF which shows the exponential drop in the abundance of LBGs beyond this magnitude, making the fraction $x_{Ly\alpha}$ at the brightest bin sensitive to rise at large values even for a low number of detected LBGs with strong Lyman- α emission. On aver-

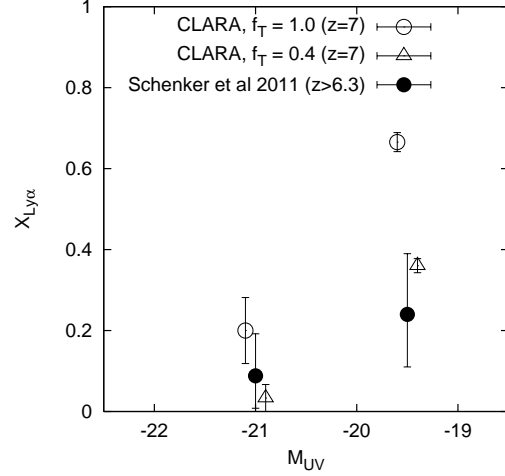


Figure 2. Same as Figure 1. Filled symbols represent the observational results by Schenker et al. (2011) for LBGs at $z > 6.3$ with Lyman- α emission with $EW > 25$ Å. The empty symbols represent our results from the simulation at $z \sim 7$. The theoretical data-points have been shifted by ± 0.1 in redshift for clarity. The first scenario (circles) corresponds to the results of our model that do not include any evolution in the absorption model at $z \sim 7$ ($f_T = 1.0$), while the second (triangles) adds a further dimming each of LAE by a factor of $f_T = 0.4$. The factor was chosen to bring our results into agreement with the observed LAE LF at $z \sim 6.5$ (Kashikawa et al. 2006). This scenario provides an improved match with the results reported by Schenker et al. (2011).

age, a fraction $x_{Ly\alpha} = 0.47 \pm 0.01$ of the galaxies between $-20.5 < M_{UV} < -18.5$ show strong Lyman- α emission with $EW > 50$ Å, where only statistical (poissonian) errors have been considered in this estimate.

3.2 Evolution at $z > 6$

Recently, results of new line searches with deep Keck spectroscopy of 19 LBGs in the redshift range $6.3 < z < 8.8$ selected with WFC3/IR data have been published (Schenker et al. 2011). The spectroscopic exposures were designed to reach EW lower than 50 Å. Under these conditions, only 2 LAEs are convincingly detected. These results suggest a strong evolution with respect to the observations at $5 < z < 6$. Using complementary observational results from ultra-deep optical spectroscopy with FORS2 on the Very Large Telescope (VLT) (Fontana et al. 2010), together with the results already obtained at $z \sim 6$ (Stark et al. 2011), the authors derive a fraction of LAEs with $EW > 25$ Å: $x_{Ly\alpha} = 0.088^{+0.088}_{-0.74}$ ($-21.75 < M_{UV} < -20.25$) and $x_{Ly\alpha} = 0.24 \pm 0.15$ ($-20.25 < M_{UV} < -18.75$). It is important to keep in mind that these fractions (estimated from the measurements at $6.3 < z < 8.8$) are based on an extrapolation of the EW distributions at redshift $z = 6$.

In Fig. 2 we present the results of our model for the $x_{Ly\alpha}$ fraction ($EW > 25$ Å) from the calculations with $f_T = 1.0$ (i.e. no evolution from the $z = 6$ extinction model) and

$f_T = 0.4$. We recall (see the final paragraph of §2.6) that the factor f_T is introduced to tune the spatial abundance of LAEs at $z = 7$ with respect to the LF inferred from observations

Both models ($f_T = 1$ and $f_T = 0.4$) yield a similar trend with M_{UV} as the one found in $5 \leq z \leq 6$. The fraction of LBGs with large EW increases for LBGs. However, the model that matches the LAE LF at $z \sim 7$ with $f_T = 0.4$ provides results for the $x_{Ly\alpha}$ fraction closer to the results derived from observations by Schenker et al. (2011) with $x_{Ly\alpha} = 0.03 \pm 0.03$ ($-21.75 < M_{UV} < -20.25$) and $x_{Ly\alpha} = 0.37 \pm 0.01$ ($-20.25 < M_{UV} < 18.75$).

4 DISCUSSION

In the previous sections we have presented a model for LBGs and LAEs that reproduce the observed trends for the $x_{Ly\alpha}$ fraction in two important aspects: 1) the rise of $x_{Ly\alpha}$ for fainter M_{UV} magnitude at a fixed redshift and 2) the overall evolution as a function of redshift between $5 \leq z \leq 7$. In this Section we discuss the key elements in our model behind these results.

4.1 Dependence of $x_{Ly\alpha}$ on M_{UV}

Assuming that the UV continuum and the Lyman- α come from star formation, one can express the intrinsic luminosities as a function of the star formation rate: $L_{\lambda UV} = 1.4 \times 10^{40} \times \text{SFR}/(\text{M}_{\odot}\text{yr}^{-1}) \text{ erg s}^{-1} \text{ \AA}^{-1}$ and $L_{Ly\alpha} = 1.9 \times 10^{42} \times \text{SFR}/\text{M}_{\odot}\text{yr}^{-1} \text{ erg s}^{-1}$ (Kennicutt 1998). The exact conversion factors depend on the IMF and the metallicity of the stellar population. We will take these values as constant, although this approximation is not fundamental in the argument that follows.

Under these assumptions, the intrinsic equivalent width (EW_i) is constant for all galaxies, $EW_i \sim 135 \text{ \AA}$, making all bright LBGs detectable as strong LAEs regardless of M_{UV} if one applies the EW cut $> 50 \text{ \AA}$. The fact that only a fraction of bright LBG are also strong LAEs can be understood as a variation of the observed EW values from the intrinsic EW_i . This is naturally expected in the presence of extinction and/or preferential scattering of Lyman- α photons out of the line of sight.

We can assume that extinction reduces the intensity of the line by a factor f_{α} and the UV continuum by a factor f_c . Further dimming by the neutral IGM can also reduce the Lyman- α line intensity by a factor \mathcal{T}_{IGM} . In this case, the measured equivalent width is $EW = \mathcal{T}_{IGM} \times (f_{\alpha}/f_c) \times EW_i$. In our model we have taken \mathcal{T}_{IGM} to be constant for all galaxies at a given redshift. Under this assumption the properties of the EW distribution can be attributed to the scatter in the extinction factors f_c and f_{α} ².

Observationally, the factor f_c can be inferred from the UV spectral slope, β . In the observed LBGs at $z > 5$ (Bouwens et al. 2010; Dunlop et al. 2011) and in our model as well, the evolution of the mean β slope at a given magnitude M_{UV} is not strong, despite the presence of considerable

scatter. On the other hand, the factor f_{α} can vary at least by a factor of 10 depending on the properties of the galaxy (Forero-Romero et al. 2011). This suggests that, at a fixed redshift, the key physical factor in our model accounting for the trend of $x_{Ly\alpha}$ with M_{UV} is the dependence of the Lyman- α escape fraction on galaxy luminosity.

To test this assumption, we show in the left panel of Fig. 3 the results of approximating the Lyman- α escape fraction, f_{α} , as a constant value. To construct this figure we keep the results for the UV continuum fixed and reduce the Lyman- α emission for all galaxies by a constant value $f_{\alpha} = 0.2$, a choice that also brings the LF for LAEs into agreement with observations at $z \sim 5$ and $z \sim 6$. This model fails to reproduce the observational trends for $x_{Ly\alpha}$, in particular it seriously underestimates the fraction of bright LAEs for faint LBGs to be $x_{Ly\alpha} = 0.10 \pm 0.01$. The Lyman- α escape fraction is too low for faint LBG, reducing too much the equivalent width and making most of these galaxies undetectable as LAEs.

To further illustrate our point, we have also implemented a phenomenological model where the f_{α} escape fraction is calculated from an effective optical depth to Lyman- α line photons, which is assumed to be proportional to the continuum optical depth,

$$f_{\alpha} = \frac{1 - \exp(-\gamma\tau_d)}{\gamma\tau_d}, \quad (6)$$

where $\gamma > 1$ and τ_d is the continuum optical depth at a wavelength of 1216 \AA . Shimizu et al. (2011) have recently applied this model to reproduce the properties of LAEs at $z = 3.1$. In Fig. 3 we show the results for $\gamma = 50$, this value was chosen to give a close match to the LAE LF at $z \sim 5$ and $z \sim 6$. This model includes a dependence of the f_{α} escape fraction on galaxy gaseous mass (and hence luminosity), via the dependence on the gas optical depth that is larger for luminous systems.

This approximation manages to reproduce similar results for $x_{Ly\alpha}$ as our radiative transfer motivated model, a result that is not surprising given the fact that the functional form of Eq.(6) is close to the expected from radiative transfer effects of the Lyman- α line in the presence of neutral Hydrogen (Hansen & Oh 2006; Forero-Romero et al. 2011).

The result from this phenomenological model adds support to our claim that the key factor in our model behind the shape of the $x_{Ly\alpha}$ - M_{UV} plot is the mass dependence of the Lyman- α escape fraction that makes luminous galaxies have, on average, small values $f_{\alpha} < 0.2$ while fainter galaxies have large $f_{\alpha} > 0.2$.

4.2 The evolution of $x_{Ly\alpha}$ beyond $z > 6$

Different authors report a change in the properties of LAE emitting galaxies beyond redshift $z > 6$, both in the LF (Hayes et al. (2011) and references therein) and the $x_{Ly\alpha}$ fraction (Schenker et al. 2011).

In our model, the drop in the LAE abundance at $z \sim 6.5$ (Kashikawa et al. 2006) and the evolution of $x_{Ly\alpha}$ at $z > 6.3$ (Schenker et al. 2011) are explained by the evolution in the IGM transmission fraction. Such evolution in the transfer of the Lyman- α line is required in our model to match the observational constraints. The dimming of all LAEs at $z \sim 7$

² Although extreme values of the EW can be used to infer the presence of unusual stellar populations (Dijkstra & Westra 2010)

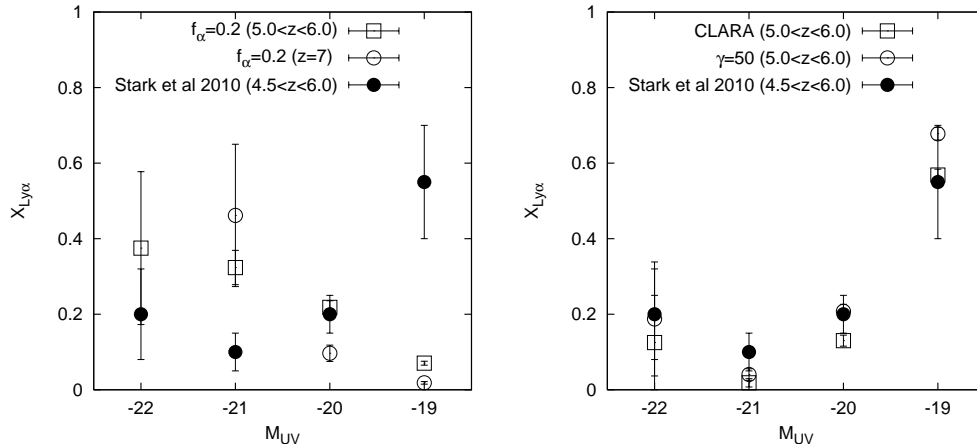


Figure 3. Same as Fig. 1 for two different models of the Lyman- α escape fraction. In both cases we keep the results for the M_{UV} magnitudes fixed and vary the Lyman- α escape fraction. The upper panel shows the results of a constant escape fraction $f_{\alpha} = 0.2$, which clearly present a trend in contradiction with the observational constraints from Stark et al. (2010). The lower panel shows the results of the model based on radiative transfer results (squares) compared against a phenomenological model where the Lyman- α escape fraction is calculated by Eq.6 (circles). The phenomenological approach shows a trend similar to the one obtained the radiative transfer model.

by a constant factor $f_T = 0.4$ makes the results of our model to better fit the LAE LF at $z \sim 6.5$ and the $x_{Ly\alpha}$ fraction at $z > 6.3$.

If confirmed, the observational evidence for a decrease in the observed $x_{Ly\alpha}$ fraction at redshifts $z > 6$ can be attributed to three reasons:

- 1) an increase in the extinction in galaxies ISM
- 2) evolution in the Hydrogen neutral fraction in the IGM
- 3) an increase in the escape fraction of ionizing photons.

Given the observational and theoretical results for UV continuum slopes for $z > 6$ (Bouwens et al. 2010; Dunlop et al. 2011; Forero-Romero et al. 2010) it is rather implausible that the extinction has increased. Therefore, only the explanations 2) and 3) seem more plausible. It is beyond scope of this paper to distinguish between these two scenarios.

However, if we add up the fraction f_T to the full transmission effect through a neutral IGM we have $\mathcal{T}_{IGM}(z = 7.0) = f_T \times 0.5 = 0.2$, where 0.5 corresponds to the fiducial value for the IGM transmission used in our model. The interpretation of this fraction $\mathcal{T}_{IGM} = 0.2$ in terms of a global neutral fraction X_{HI} is considerably more difficult. Different models can give results in the range $X_{HI} \sim 0.4 - 0.9$ depending on the treatment of the line through the IGM, making it difficult to rule out large values of the neutral HI fraction from the evolution in $x_{Ly\alpha}$, specially when gas bulk velocities from winds are included in the analysis (McQuinn et al. 2007; Dijkstra et al. 2011).

5 CONCLUSIONS

Observations report that not all bright Lyman Break Galaxies in the redshift range $5 \leq z \leq 7$ are seen as strong Ly-

man Alpha Emitters (Stark et al. 2010, 2011; Fontana et al. 2010; Schenker et al. 2011). The fraction of LBGs that can be detected with strong Lyman- α emission, $x_{Ly\alpha}$ tests the equivalent width distribution, providing additional information that is not included in the luminosity function of LAEs and LBGs. In this paper we present a theoretical model of high redshift LBGs and LAEs that reproduce the observed trends for $x_{Ly\alpha}$ in the redshift range $5 \leq z \leq 7$. We find that the a decreasing Lyman- α escape fraction with increasing galaxy luminosity is a key element in our model to explain the observations.

In the redshift range $5 \leq z \leq 6$ observations show a clear evolution of the $x_{Ly\alpha}$ with absolute magnitude M_{UV} . From the results of our model, we suggest that a key ingredient to explain this trend is the decrease of the Lyman- α escape fraction with increasing galaxy luminosity. We test this hypothesis by fixing the UV continuum results and assuming a constant value for f_{α} . This produces an increasing fraction of LBGs with strong Lyman- α emission for brighter M_{UV} , the exact opposite trend of what is reported by observations. In contrast, a model with a decreasing Lyman- α escape fraction with increasing galaxy mass can simultaneously reproduce the observed trends for $x_{Ly\alpha}$ and the LAE-LF. The additional influence of an IGM transmission coefficient, \mathcal{T}_{IGM} , dependent on large scale environment (Zheng et al. 2011) is a point that deserves further investigation. In particular, it would be useful to know to what extent this kind of environment dependent transmission explains the trend of $x_{Ly\alpha}$ with absolute magnitude M_{UV} .

In order to reproduce the $x_{Ly\alpha}$ evolution at $z > 6.3$ our model requires a decrease of the transmission fraction of Lyman- α photons by a factor of $f_T = 0.4$, also improving the agreement with the observed LAE LF at $z \sim 6.5$, although confirmation of such evolution from increased sensitivity observations and larger samples is still needed.

The fraction $x_{\text{Ly}\alpha}$ provides an additional statistical tool to describe galaxy populations evolving during the reionization epoch. More sensitive instruments and larger galaxy samples will be necessary to quantify the evolution of the $x_{\text{Ly}\alpha}$ fraction. In the same spirit, this statistic can be used as a benchmark for a theoretical model aiming at describing the evolving galaxy populations at these redshifts.

ACKNOWLEDGMENTS

We thank the anonymous referee for the careful reading and the thoughtful comments which helped us to improve the clarity of the paper. We thank Matthew Schenker for providing us with the results from his paper in electronic format, and for useful clarifications on the procedure to calculate the $x_{\text{Ly}\alpha}$ fraction.

The simulation used in this work is part of the MareNostrum Numerical Cosmology Project at the BSC. The data analysis has been performed at the NIC Juelich and the LRZ Munich.

JEFT and FP acknowledge the support by the ESF ASTROSIM network through the short visit grant scheme that helped in the development process of CLARA.

GY acknowledges support of MICINN (Spain) through research grants FPA2009-08958 and AYA2009-13875-C03-02. We equally acknowledge funding from the Consolider project MULTIDARK (CSD 2009-00064) and the Comunidad de Madrid project ASTROMADRID (S2009/ESP-146).

REFERENCES

- Atek H., Kunth D., Hayes M., Östlin G., Mas-Hesse J. M., 2008, *A&A*, 488, 491
- Bouwens R. J., Illingworth G. D., Oesch P. A., Trenti M., Stiavelli M., Carollo C. M., Franx M., van Dokkum P. G., Labbé I., Magee D., 2010, *ApJL*, 708, L69
- Charlot S., Fall S. M., 2000, *ApJ*, 539, 718
- Dayal P., Maselli A., Ferrara A., 2011, *MNRAS*, 410, 830
- Devriendt J. E. G., Guiderdoni B., Sadat R., 1999, *A&A*, 350, 381
- Dijkstra M., Lidz A., Wyithe J. S. B., 2007, *MNRAS*, 377, 1175
- Dijkstra M., Mesinger A., Wyithe J. S. B., 2011, *MNRAS*, 414, 2139
- Dijkstra M., Westra E., 2010, *MNRAS*, 401, 2343
- Dunlop J. S., McLure R. J., Robertson B. E., Ellis R. S., Stark D. P., Cirasuolo M., de Ravel L., 2011, *ArXiv e-prints*
- Fontana A., Vanzella E., Pentericci L., Castellano M., Giallisco M., Grazian A., Boutsia K., Cristiani S., Dickinson M., Giallongo E., Maiolino R., Moorwood A., Santini P., 2010, *ApJL*, 725, L205
- Forero-Romero J. E., Yepes G., Gottlöber S., Knollmann S. R., Cuesta A. J., Prada F., 2011, *MNRAS accepted*
- Forero-Romero J. E., Yepes G., Gottlöber S., Knollmann S. R., Khalatyan A., Cuesta A. J., Prada F., 2010, *MNRAS*, 403, L31
- Guiderdoni B., Rocca-Volmerange B., 1987, *A&A*, 186, 1
- Hansen M., Oh S. P., 2006, *MNRAS*, 367, 979
- Hatton S., Devriendt J. E. G., Ninin S., Bouchet F. R., Guiderdoni B., Vibert D., 2003, *MNRAS*, 343, 75
- Hayes M., Schaerer D., Östlin G., Mas-Hesse J. M., Atek H., Kunth D., 2011, *ApJ*, 730, 8
- Iliev I. T., Shapiro P. R., McDonald P., Mellema G., Pen U.-L., 2008, *MNRAS*, 391, 63
- Kashikawa N., Shimasaku K., Malkan M. A., Doi M., Matsuda Y., Ouchi M., Taniguchi Y., Ly C., Nagao T., Iye M., Motohara K., Murayama T., Murozono K., Nariai K., Ohta K., Okamura S., Sasaki T., Shioya Y., Umemura M., 2006, *ApJ*, 648, 7
- Kennicutt Jr. R. C., 1998, *ARA&A*, 36, 189
- Knollmann S. R., Knebe A., 2009, *ApJS*, 182, 608
- Kunth D., Mas-Hesse J. M., Terlevich E., Terlevich R., Lequeux J., Fall S. M., 1998, *A&A*, 334, 11
- Laursen P., Sommer-Larsen J., Razoumov A. O., 2011, *ApJ*, 728, 52
- Leitherer C., Schaerer D., Goldader J. D., González Delgado R. M., Robert C., Kune D. F., de Mello D. F., Devost D., Heckman T. M., 1999, *ApJS*, 123, 3
- Mathis J. S., Mezger P. G., Panagia N., 1983, *A&A*, 128, 212
- McQuinn M., Hernquist L., Zaldarriaga M., Dutta S., 2007, *MNRAS*, 381, 75
- Meiksin A., 2006, *MNRAS*, 365, 807
- Osterbrock D. E., 1989, *Astrophysics of gaseous nebulae and active galactic nuclei*
- Schenker M. A., Stark D. P., Ellis R. S., Robertson B. E., Dunlop J. S., McLure R. J., Kneib J., Richard J., 2011, *ArXiv e-prints*
- Shimizu I., Yoshida N., Okamoto T., 2011, *ArXiv e-prints*
- Spergel D. N., Verde L., Peiris H. V., Komatsu E., Nolte M. R., Bennett C. L., Halpern M., Hinshaw G., Jarosik N., Kogut A., Limon M., Meyer S. S., Page L., Tucker G. S., Weiland J. L., Wollack E., Wright E. L., 2003, *ApJS*, 148, 175
- Springel V., 2005, *MNRAS*, 364, 1105
- Springel V., Hernquist L., 2003, *MNRAS*, 339, 289
- Stark D. P., Ellis R. S., Chiu K., Ouchi M., Bunker A., 2010, *MNRAS*, 408, 1628
- Stark D. P., Ellis R. S., Ouchi M., 2011, *ApJL*, 728, L2+
- Verhamme A., Schaerer D., Maselli A., 2006, *A&A*, 460, 397
- Zheng Z., Cen R., Trac H., Miralda-Escudé J., 2010, *ApJ*, 716, 574
- Zheng Z., Cen R., Trac H., Miralda-Escudé J., 2011, *ApJ*, 726, 38